Numerical and experimental analysis of a 3D printed Savonius rotor with built-in extension plate

Burcin Deda Altan[*1], Volkan Kovan[2] and Gurkan Altan[1]

[1]*Faculty of Engineering, Department of Mechanical Engineering, Pamukkale University, Kinikli 20070 Denizli, Turkey*
[2]*Faculty of Engineering, Department of Mechanical Engineering, Akdeniz University, Antalya, Turkey*

Abstract. In this study, the enhancement of the conventional Savonius wind rotor performance with extension plate has been investigated experimentally and numerically. Experimental models used in the study have been produced with 3D (three dimensional) printing, which is one of the rapid prototyping techniques. Experiments of produced Savonius wind rotor models have been carried out in a wind tunnel. CFD (Computational Fluid Dynamics) analyses have been performed under the same experimental conditions to ensure that experiments and numerical analyses are supported to each other. An additional extension plate has been used in order to enhance the performance of the conventional Savonius wind rotor with a gap distance between blades. It can be called modified Savonius rotor or Savonius rotor with built-in extension plate. Thus, the performance of the rotor has been enhanced without using additional equipment other than the rotor itself. Numerical and experimental analyses of Savonius wind rotor models with extension plate have been carried out under predetermined boundary conditions. It has been found that the power coefficient of the modified Savonius rotor is increased about 15% according to the conventional Savonius rotor.

Keywords: Savonius; wind rotor; 3D printer; performance; extension plate

1. Introduction

Developing industry has a constantly increasing need for energy. New and renewable energy sources are becoming increasingly important due to the reduction in the availability of fossil energy sources over time and environmental problems caused by them. The wind energy is one of the renewable energy sources. Wind energy has become an indispensable energy source thanks to developments in wind energy systems over time. The cost of installations that generate power using the wind energy has dropped with developments in technology. Wind rotors are the most important parts of installations that generate power using the wind energy. Studies on improving wind energy systems and increasing the efficiency of wind rotors are still going on. To this day, many different wind rotors and wind energy systems have been made, tried and used. Savonius wind rotors, which have a low aerodynamic performance, have not attracted much attention until recently although they have certain strengths when compared to other conventional wind rotors. Thus, in recent years, some researches have been made to enhance the performance of Savonius wind rotors and these efforts are still going on.

Gupta *et al.* (2008) made a combination between Savonius wind rotor and Darrieus wind rotor. They observed that there is a definite improvement in the power coefficient for the combined Savonius–Darrieus rotor.

Kamoji *et al.* (2008) studied the effect of the overlap ratio, blade arc angle, aspect ratio and Reynolds number on the performance of Savonius rotor. Saha and Rajkumar (2006) compared the performance of three-blade Savonius wind rotor twisted by a 15° twist angle with that of a classical Savonius wind rotor by conducting an experiment on them in a low-speed wind tunnel. Saha *et al.* (2006) attempted to investigate the wind tunnel tests of a two-stage Savonius rotor with semi-circular and twisted blades to assess its performance; tests are also planned for single and three-stage rotor systems. Aldoss (1984) made a change in the rotor blade and designed the swinging blade model to improve the aerodynamic performance of Savonius wind rotor, thus analysing the performance of the rotor experimentally. Ishimatsu *et al.* (2002) analysed the performance of the conventional Savonius wind rotor and Bach-type Savonius wind rotor numerically. Grinspan *et al.* (2001) tested in their experiments rotor of two different blade types, one being an airfoil type and the other twisted type, in order to improve the Savonius wind rotor design with three blades. Deda Altan and Atilgan (2010-2012) introduced a curtain arrangement without changing the basic structure of a Savonius wind rotor to improve the performance and increase the efficiency of the rotor. Akwa *et al.* (2012) discussed the influence of the buckets overlap ratio of a Savonius wind rotor on the averaged moment and power coefficients. Mohamed *et al.* (2010) studied several shapes of obstacles and deflectors placed in front of two and three blade Savonius turbine. Driss *et al.* (2014) carried out numerical simulation and experimental validation to study the turbulent flow around a small incurved Savonius wind rotor. Nasef *et al.* (2013) analysed numerically an aerodynamic performance of stationary and rotating

---

*Corresponding author, Ph.D.
E-mail: bdeda@pau.edu.tr

Savonius rotor for various overlap ratios. Goodarzi and Keimanesh (2015) proposed two large Savonius turbine to use near the radiators of a natural draft dry cooling tower instead of previously proposed solid windbreakers. Damak *et al*. (2013) experimentally investigated the effect of overlap ratio and the effect of the Reynolds number on the performance of the rotor. El-Askary et al. (2015) developed new deflector designs for capturing wind energy. They studied numerically the performance of Savonius rotor with different modifications to enhance the turbine power. Aresti *et al*. (2013) studied a numerical approach to predict performance of wind turbines. Kacprzak *et al*. (2013) numerically analysed three geometries of Savonius wind turbine rotors, namely Classical, Bach-type and Elliptical designs with constant cross-sections. Lee *et al*. (2016) investigated the performance and shape characteristics of a helical Savonius wind turbine at various twist angles. Sharma and Kumar Sharma (2017) performed numerical study on the modified configuration to study the effect of layered multiple miniature blades on the performance of Savonius rotor. Tahani *et al*. (2017) designed an innovative Savonius-style wind rotor which is capable of directing the discharge flow to utilize the flow for ventilation and produce the power for electricity demand in buildings.

This study aims to enhance the aerodynamic performance of Savonius wind rotors, which are not widely used due to their low rotor efficiency. To this end, the performance efficiency has been examined after the addition of an extension plate. In this way, a performance enhancement has been achieved with the Savonius wind rotor with built-in extension plate. A 3D printer has been used to produce modified and conventional Savonius rotors. Thus, with the improvement of the low efficiency, it is expected that the use of the Savonius wind rotor should become more widespread.

2. Savonius rotor design, performance calculations and production (3D Printer)

The Savonius wind rotor consists of two semi-cylinders are called blades placed between two horizontal discs and centers of these blades are slid symmetrical to each other. Wind striking to the Savonius wind rotor at a certain speed generates a positive torque in the inner part of the cylinder and a negative torque on the outer part of the cylinder. The torque generated in the inner part of the cylinder is greater than the torque generated on the outer part, which provides a rotational motion.

The design parameters of the Savonius wind rotor have been determined taking into account previous studies in the literature and the dimensions of the wind tunnel used in the experiment. Accordingly; end plate diameter has been taken as $D_o = 1.1 \times D$. Here, D_o represents the end plate diameter and D represents the rotor diameter. As shown in Fig. 1, the rotor diameter is D=12 cm, the rotor height is H=20 cm and upper and lower end plate diameters are D_o=13.2 cm. Reviewing previous studies in the literature, G=(e/d) overlap ratio has been determined as another design parameter. Here, e represents the gap distance and d

represents the blade diameter. In this study, the gap distance has been taken as e=1.6 cm according to the previous literatures' optimum values (Deda Altan and Atilgan 2010) and the blade diameter has been taken as d=2r=6.8 cm.

An additional extension plate has been used to increase the performance of the Savonius wind rotor. The additional extension plate has been attached tangentially to the end of the rotor's blade as shown in Fig. 2. The extension plate has been planned as a whole with the rotor's blade, thus they have been produced together. Here, the extension plate length has been taken as L and the plate radius has been taken as r. The height of the extension plate has been accepted to be the same with the rotor height. The optimum extension plate length has been found by performing analyses in different ratios of the extension plate length to the blade radius.

For the purposes of the Savonius wind rotor performance calculation, the rotor end speed ratio is calculated as follows
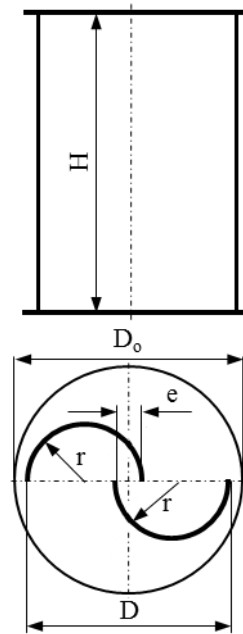
$$\lambda = \frac{w.D}{2.V} \qquad (1)$$
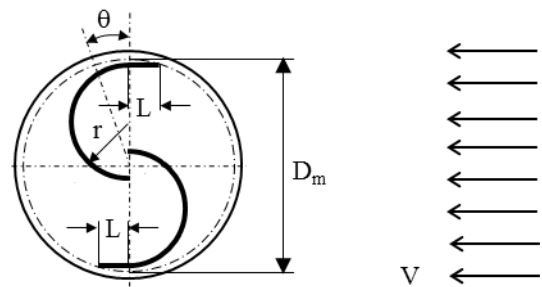

Fig. 1 Geometric parameters of the Savonius rotor

Fig. 2 Savonius wind rotor with built-in extension plate

Here, w represents the angular speed of the rotor, V represents the speed of wind and D represents the rotor diameter. Rotor diameter (D) should be taken as modified rotor diameter (D_m) in the modified rotors as shown in Fig. 2. The reason is that the extension plate length leads to the expansion of the rotating rotor diameter. The modified rotor diameter of the maximum rotated projected area used in calculations has been found with the help of the drawing program. Thus, the rotor diameter (D) has been used in the calculations of the conventional Savonius rotor and also the modified rotor diameter (D_m) has been used in the calculations of the modified Savonius rotor. The static torque coefficient (C_{ts}) and the coefficient of power (C_p) of the rotor are as follows

$$C_{ts} = \frac{4.T_s}{\rho.H.D^2.V^2} \qquad (2)$$

$$C_p = \frac{2.T.w}{\rho.H.D.V^3} \qquad (3)$$

Here, T_s represents the static torque obtained from the rotor, T represents the dynamic torque obtained from the rotor and ρ represents the air density.

The Savonius wind rotor models used in the experimental part of the study have been produced with a 3D printer using the FDM (Fused Deposition Modeling) technique as shown in Fig. 3. The CAD (Computer-aided design) model of the conventional Savonius wind rotor designed on computer can be seen in Fig. 3(a) and the Savonius wind rotor produced with a 3D printer can be seen in Fig. 3(b). Printing with a 3D printer is the process of making a three dimensional solid object from a digital three dimensional (CAD) file. Although 3D Printers show differences among themselves, they have the same principles. The 3D printer adds the next layer on top of each layer until the final object is produced. In 3D printers; ABS (Acrylonitrile butadiene styrene), PLA (poly lactic acid), and other similar plastic raw materials are melted to create layers. The 3D printer used in this study feeds the PLA filament to the extrusion head. Here, the material is heated and melted. The extrusion head can move with the help of the computer-aided manufacturing (CAM) software on 2 axes and eject the molten material on an empty tray to form the first layer. The tray moves down a step with each layer and thus the part is built in layers. Sprayed material solidifies instantly and the part is removed from the tray when the construction of all layers is completed.

3. Experimental analysis

A wind tunnel with a circular exit has been used in experiments performed with the Savonius wind rotor. The speed of wind at the test section of the wind tunnel can optionally be changed between 11-40 m/s with an adjustable damper. The test section has a length of 610 mm and a cross-section of 305 mm x 305 mm. The wind tunnel used in the experiments has a turbulence intensity of around

1% and a flow uniformity of around 1%. The test section has been built using transparent polycarbonate plates and mounted to the wind tunnel with bolts. The Savonius wind rotor has been set up on the test section shown in Fig. 4.

In order to ensure that the rotor is mounted firmly in the tunnel, housings have been opened at the center of the upper and lower blade tip plate so that the metal shaft with a bearing at one tip could be mounted. In this way, the desired (e) gap distance has been achieved between the blades. In order to reduce friction forces, the shaft of the Savonius wind rotor has been supported at the top and bottom with bearings with very low friction. Deep groove ball bearings as bearings have been used also for being robust in operation, requiring little maintenance.
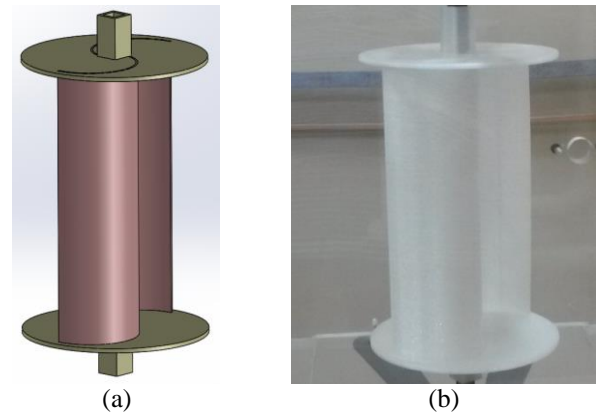

(a)   (b)

Fig. 3 (a) CAD Model of Savonius wind rotor and (b) Produced Savonius wind rotor
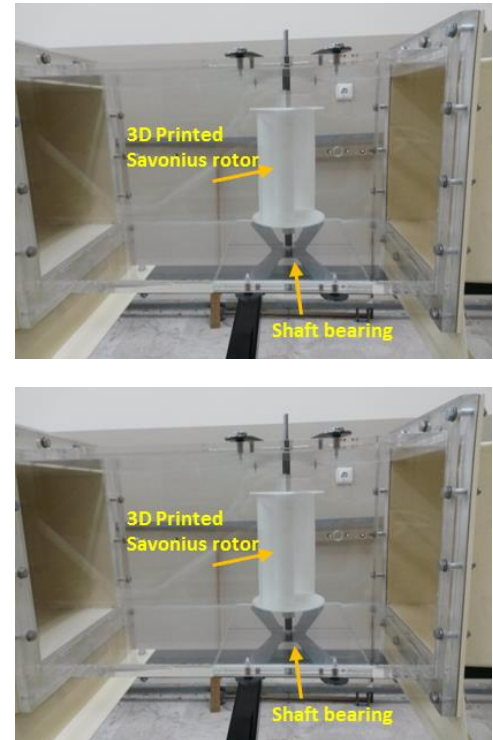

Fig. 4 Test section of Savonius rotor

TESTO 435 multifunctional anemometer, which has a wind speed measurement range of 0.6-40 m/s, has been used in order to measure the speed of wind. The accuracy of multifunctional anemometer is ±0.2 m/s. The experiments have been carried out at a wind speed of 11 m/s. IMADA HGT-10 torque meter sensor with a measuring range of 0–10 Nm has been used to measure the static torque that forms on the Savonius wind rotor shaft. The accuracy of torque meter sensor is ±0.5%. An angle gauge has been used to obtain the torque from the desired angle of the rotor. The uncertainties of parameters obtained from experimental study have been calculated as R_e = 2.34%, C_{ts} = 6.9%, λ = 2.18% and C_p = 7.3% (Binici 2001, Genceli 1998).

The effect of blockage is an important condition that needs to be examined in a wind tunnel. The ratio of maximum projected area of the wind rotor model to the cross-sectional area of the wind tunnel is blockage ratio ($B_R=S_a/T_a$). Accordingly, this ratio has been found in the value of 25%. The adapted Maskell's blockage correction method is produced well corrected results for the Savonius wind rotor (Hayashi *et al.* 2005, Ross *et al.* 2011 and Chen and Liou 2011). Thus, all data obtained from the study have been corrected considering this blockage correction method.

4. Numerical analysis

Ansys workbench with Fluent program has been used for numerical analysis. Fluent is Computational Fluid Dynamics (CFD) software which employs the finite volume method. Static and aerodynamic values have been obtained via numerical analysis. The numerical analysis has been carried out under steady state conditions. The steady state CFD analysis has been used to analyse the static performances and the aerodynamic performance of the rotors in terms of power and torque coefficients. A series of steady state simulations have been performed to obtain the each relevant value of aerodynamic performance.

As shown in Fig. 5, the study has been modelled with the required boundary conditions. The dimensions of numerical study domain have been taken same with experimental set up. The test section of wind tunnel with the turbulence intensity less than 1% has been simulated in the numerical analysis. The numerical study domain has been formed with rotating and fixed flow zones. An interface has been prepared so that the rotating zone and the fixed flow zone could interact in rapport. Thus, the numerical study has been solved using the sliding mesh model. The velocity inlet condition has been chosen to be 11m/s and the pressure output condition has been chosen to be the atmospheric pressure because of that the exit of tunnel is in the outside of laboratory. The air considered in this study is an incompressible fluid. The Reynolds number used in this study is $2.2.10^5$ for experimental and numerical analysis. Therefore, the flow around the Savonius rotor is turbulent. There are several turbulence models to numerically solve the flow field around the Savonius wind rotor. The best turbulence model is the model that yields the closest result to the results obtained from the experiments. The k-ε, RSM (Reynolds stress model) and LES (Large eddy simulation) turbulence models are primary valid for turbulent core flows. Spalart-Allmaras and k-ω are valid throughout the boundary layer. It can be observed that the affected region with their corresponding wall y^+, namely the: viscous sublayer region (y^+<5), buffer region (5<y^+<30), fully turbulent or log-law region (30<y^+<300). The production of fine mesh near the wall reduces the values of y^+, but increases the number of nodes and hence the computational time. Larger values of y^+ are recommended when using wall functions. Wall functions are used with Standard k-ε model for the near wall treatment. The standard k-ε turbulence model has been preferred according to the other all turbulence models' advantages and disadvantages. It has been selected as the turbulence model most compatible with the experimental results. At the same time, it is advantageous that the computational time is short. A y^+ study has been also carried out to choose the best desired y^+ value for the Standard k-ε model. The values of y^+ have been selected as 37, 57, 77, 100 at the same velocity. Mesh structures have been produced according to these values. The best value of y^+ has been determined by comparing with the experimental data. In this study, the value of y^+ has been found 37 according to the mesh structure.

Fig. 6 shows the meshed status at the test section of the rotor. A grid independence limit study has been carried out to reduce the computational time and to be closer to the experimental data by using k-ε turbulence model. Therefore, an optimal value of mesh refinement has been found for precision and accuracy. A smaller mesh procedure has been used in the rotor area according to the overall tunnel volume in order to be in harmony with the experimental results and numerical results. Triangular pyramid shaped mesh elements have been used in the mesh formation process. According to the grid independence limit study results, the total number of mesh have been taken around 0.5 million considering the simulation time and it is determined that the obtained numerical results are in good agreement with the experimental results. The same numerical data of grid resolution have been used throughout the study. Thus, the best parameters have been obtained by comparing performance values obtained with different geometrical parameter.
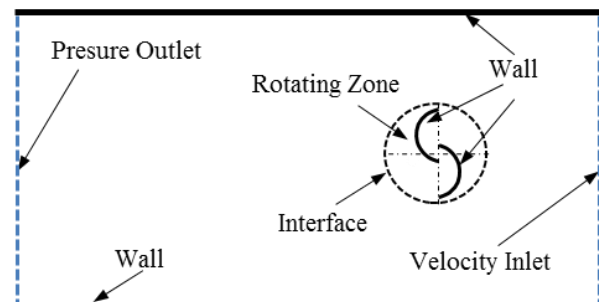

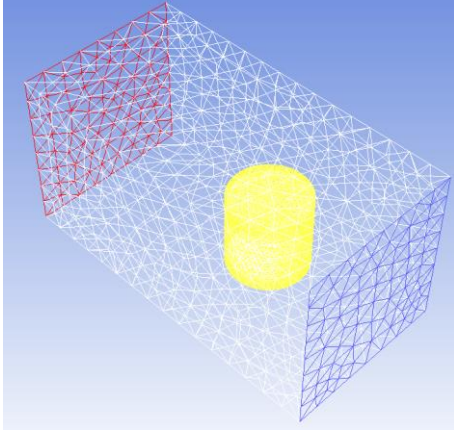Fig. 5 Numerical model of Savonius rotor

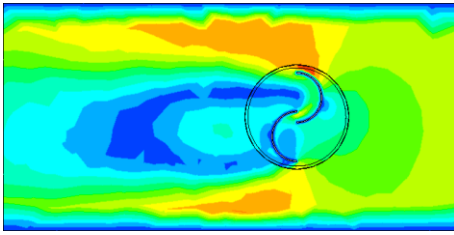Fig. 6 Meshed status at the test section of the rotor

Fig. 7 Velocity contour of test section

Experiments have been carried out in the test section of the wind tunnel. There is a contraction section in front of the test section so that the flow in the wind tunnel can uniformly arrive to the test section. Therefore, this experimental uniform velocity distribution in the test section has been also simulated. As shown in the simulation velocity contour in Fig. 7, there is no velocity gradient at the velocity inlet boundary.

Mass and momentum conservation equations that used by fluent program for the Cartesian tensor rotation for general compressible and incompressible steady flows can be written as follows:

Continuity equation

$$\frac{\partial}{\partial x_j}\left(\rho.u_j\right)=0 \tag{4}$$

Momentum equation

$$\frac{\partial}{\partial x_j}\left(\rho.u_j.u_i - \tau_{ij}\right)=\frac{\partial p}{\partial x_j}+S_i \tag{5}$$

In both these equations;

x_j : cartesian coordinate (j=1, 2, 3), u_i : absolute velocity components in the x_i direction.

p : piezometric pressure = p_s-ρ_o.g.x_m , here; p_s : static pressure, ρ_o : reference density,

g : gravitational acceleration and x_m : coordinate where ρ_o is defined.

ρ : density and τ_{ij} are the components of the stress tensor.

S_i: gravitational force = ρ.g_i

Here, the stress tensor is as follows

$$\tau_{ij} = \mu_{eff}.s_{ij} - \frac{2}{3}\mu_{eff}.\frac{\partial u_k}{\partial x_k}.\delta_{ij} \tag{6}$$

μ_{eff}=μ_l +μ_t is effective viscosity of fluid (where μ_l is laminar viscosity and μ_t is turbulent viscosity. δ_{ij} is Kronecker delta and S_{ij} is the change of the strain tensor and written as follows

$$s_{ij} = \frac{\partial u_i}{\partial x_j}+\frac{\partial u_j}{\partial x_i} \tag{7}$$

Kronecker delta if i $\neq$ j $\Rightarrow$ 0

$$\delta_{ij} = \begin{cases} 0 & (i \neq j) \\ 1 & (i = j) \end{cases} \tag{8}$$

Standard k-ε turbulence model and logarithmic surface function have been used for the solution of the turbulent flow. Momentum equation, x and y components of velocity, kinetic energy of turbulence (k) and turbulence distribution ratio (ε) have been solved by the program. All these solutions have been done by using iteration methods and secondary interpolation methods with high safety, have been used. However, in every iteration, pressure arrangement has been solved in order to protect availability of the pressure zone and mass conservation. In the calculation of pressure and velocity distribution Simple solution algorithm has been used (Deda Altan and Atilgan 2010).

5. Results and discussions

This study experimentally and numerically examines the performance of the conventional Savonius rotor and the Savonius rotor with built-in extension plate. The static torque of the Savonius rotor at different angles has been measured in the experiments. Numerical analyses have been used to examine the effect of the extension plate's length. In addition, the changes in coefficient of power have been examined and compared.

The change in the static torque coefficient and the rotor angle for the conventional Savonius rotor is shown in Fig. 8 both experimentally and numerically. The rotor angle has been manipulated from 0 degree to 360 degrees in order to determine the value of the static torque coefficient at all angles. The change in static torque coefficient between 0-180 degrees has been found to be the same with the change between 180-360 degrees. This symmetry in change has been found to be due to the two-bladed Savonius wind rotor's symmetry in design. It has been determined that positive but variable torque has been generated at all values of the rotor angle. As can be seen in the Figure, the maximum torque has been obtained at an angle around 30 and 210 degrees, while the minimum torque has been obtained around 120 and 300 degrees. It has been determined that the static data obtained from experiments

and numerical analyses coincide in harmony. Thus, the numerical analyses have been supported by the experimental data.

The conventional Savonius rotor has been improved with an additional extension plate. When determining the optimum plate size, the optimization has been carried out with numerical analysis in order to save material and time. In order to ensure data accuracy, a numerical analysis infrastructure overlapping with experiments has been used. The Savonius wind rotor with extension plate that yielded the best results has been produced and used in the experiments. The extension plate has been attached tangential to both blades. The length of the extension plate has been altered depending on the radius of the blade. Accordingly, the effect of the extension plate on torque between L/r ratio of 0.4 and 1.5 is shown in Fig. 9. The increase in torque is given in percentage of increase compared to torque values obtained from the conventional Savonius rotor. The effect of the additional extension plate on the torque generation has been examined between angles of 0-180 degrees due to the symmetry between static torque coefficients at 0-180 degrees and 180-360 degrees for the conventional Savonius wind rotor. A positive increase in torque has been found for the Savonius wind rotor with extension plate between angles of 45 and 165. At other angles, decreases have been observed due to the position of extension plate according to the incoming wind.
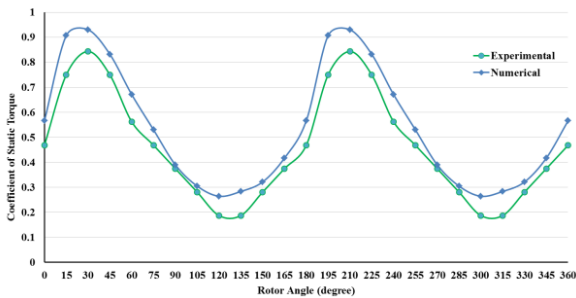

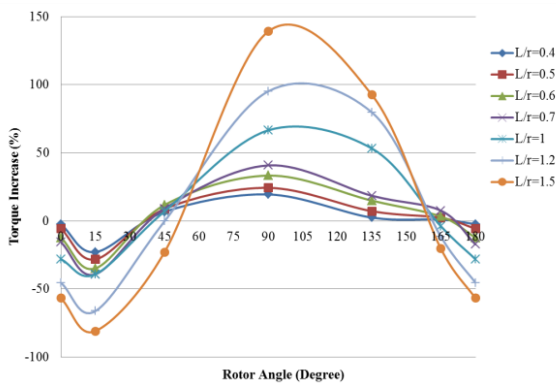Fig. 8 Coefficient of static torque for the conventional Savonius rotor

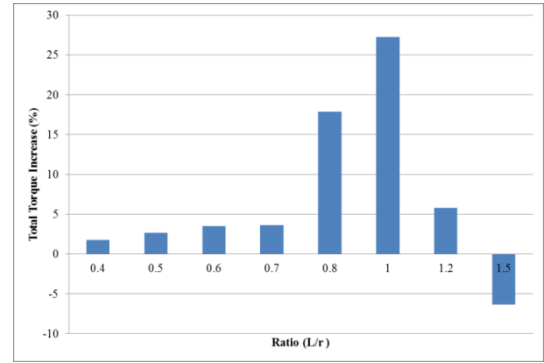Fig. 9 Effects of the extension plate on the torque increase

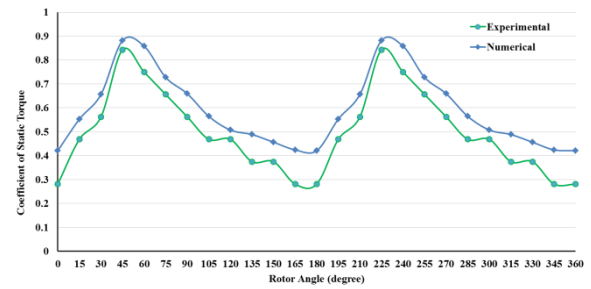Fig. 10 Effects of the L/r ratio on the total torque increase

Fig. 11 Coefficient of static torque for the modified Savonius rotor

The total torque increases obtained from rotor according to the L/r ratio are given in Fig. 10. As can be seen in the Figure, all L/r ratios have been resulted in an increase in the total torque except for 1.5. It has been determined that the increase in the total torque continued until the L/r ratio of 1 and started to decrease after this value. The maximum increase in total torque has been found about 26% and at the L/r ratio of 1. Since the efficiency of the rotor increases in line with the increase in the total torque, the L/r ratio has been taken as 1 and the Savonius wind rotor with extension plate to be used in the experimental study has been produced using this value.

Thus, the conventional Savonius wind rotor has been improved with an additional extension plate. The optimum rotor with built-in extension model determined as a result of numerical development study has been produced with a 3D printer and its performance has been assessed both experimentally and numerically. Fig. 11 shows the change in the static torque coefficient according to the rotor angle of the improved conventional Savonius rotor. The maximum positive torque has been obtained at the angles of 45 and 225 degrees for the improved conventional Savonius rotor. It has been found that the obtained numerical data have been consistent with the experimental data. The maximum torque for the rotor with extension plate has been obtained at 15 degrees higher compared to the conventional Savonius rotor. In other words, it has been found that the improved rotor generated a higher torque from 45 degrees to 165 degrees compared to the conventional rotor. Thus, rotor angles that produce a higher positive torque have been achieved with the use of an extension plate.
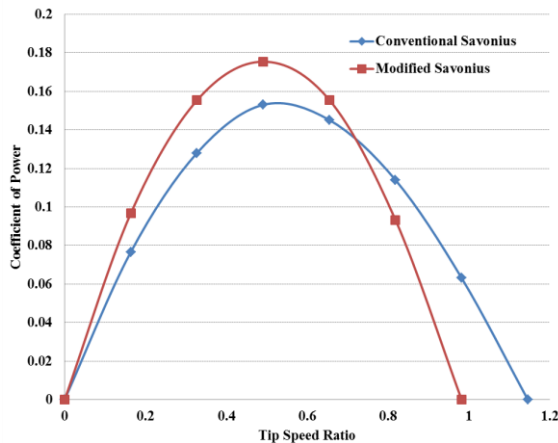
Fig. 12 Change of coefficient of power

Fig. 12 shows the change in the coefficient of power according to the tip speed ratio for both conventional and the modified Savonius rotor. The change in the coefficient of power has been obtained via numerical analysis. There is difference of about 6% between idle rotation speeds of both rotors, which indicates a good fit. Thus, the experimental data and the numerical data have supported each other in terms of idle rotation speed as well. It has been found that the tip speed ratio of the maximum coefficient of power is 0.5 for both Savonius rotors. It has been found that the coefficient of power of the Savonius rotor with extension plate increased, while its tip speed ratio slightly decreased. It has been found that the coefficient of power of the Savonius rotor with extension plate is approximately 15% higher than the conventional Savonius rotor. The maximum power coefficient of the conventional Savonius-type rotor has been found about15%. When the literature has been reviewed, the maximum power coefficient obtained from the study has been determined between the values of in the literature to be identified (Fujisawa and Gotoh 1994, Tong *et al.* 2013).

6. Conclusions

In this study, static and dynamic performance analyses of the conventional and the modified Savonius rotor have been carried out both numerically and experimentally. Results of the experimental and numerical analyses have been compared.

1. The conventional and the improved Savonius wind rotor models have been produced with the new 3D printer technology under laboratory conditions and within a short amount of time. In this way, experimental studies have been performed with rapid prototyping.

2. The change in the static torque coefficient according to the rotor angle has been examined both experimentally and numerically for the conventional and the modified Savonius rotor. It has been found as a result of these examinations that experiments have been consistent with numerical analyses; therefore the numerical study has been

supported by the experimental analysis.

3. It has been found that idle rotation speed of the tip speed ratio, which is performance parameters of the Savonius rotor, have supported each other both experimentally and numerically.

4. The optimum additional extension plate parameter has been found to be (L/r) ratio = 1.

5. It has been found that the improved rotor generated a higher torque from 45 degrees to 165 degrees compared to the conventional rotor. Thus, rotor angles that produce a higher positive torque have been achieved with the use of an extension plate.

6. It has been found that the coefficient of power of the improved Savonius rotor is approximately 15% higher than the conventional Savonius rotor.

References

Akwa, J.V., Junior, G.A. and Petry, A.P. (2012), "Discussion on the verification of the overlap ratio influence on performance coefficients of a Savonius wind rotor using computational fluid dynamics", *Renew. Energ.*, **38**, 141-149.

Aldoss, T.K. (1984), "Savonius rotor using swinging blades as an augmentation system", *Wind Eng.*, **8**(4), 214-220.

Aresti, L., Tutar, M., Chen, Y. and Calay, R.K. (2013), "Computational study of a small scale vertical axis wind turbine (VAWT): comparative performance of various turbulence models", *Wind Struct.*, **17**(6) 647-670.

Binici, I. (2001), "Industrial measurement and calibration", Birsen Press, Istanbul.

Chen, T.Y. and Liou, L.R. (2011), "Blockage corrections in wind tunnel tests of small horizontal-axis wind turbines", *Exp. Therm. Fluid Sci.*, **35**(3), 565-9.

Damak, A., Driss, Z. and Abid, M.S. (2013), "Experimental investigation of helical Savonius rotor with a twist of 180", *Renew. Energ.*, **52**, 136-142.

Deda Altan, B. and Atilgan, M. (2010), "The use of a curtain design to increase the performance level of a Savonius wind rotors", *Renew. Energ.*, **35**, 821-829.

Deda Altan, B. and Atilgan, M. (2012), "A study on increasing the performance of Savonius wind rotors", *J. Mech. Sci. Technol.*, **26**(5), 1493-1499.

Driss, Z., Mlayeh, O., Driss, D., Maaloul, M. and Abid, M.S. (2014), "Numerical simulation and experimental validation of the turbulent flow around a small incurved Savonius wind rotor", *Energy*, **74**, 506-517.

El-Askary, W.A., Nasef, M.H., AbdEL-hamid, A.A. and Gad, H.E. (2015), "Harvesting wind energy for improving performance of Savonius rotor", *J. Wind Eng. Ind. Aerod.*, **139**, 8-15.

Fujisawa, N. and Gotoh, F. (1994), "Experimental study on the aerodynamic performance of a Savonius rotor", *J. Solar Energ. Eng.*, **116**(3), 148-152.

Genceli, O.F. (1998), "Measurement technique", Birsen Press, Istanbul.

Goodarzi, M. and Keimanesh, R. (2015), "Numerical analysis on overall performance of Savonius turbines adjacent to a natural draft cooling tower", *Energ. Convers. Manage.*, **99**, 41-49.

Grinspan, A.S., Kumar, P.S., Saha, U.K., Mahanta, P. Ratna Rao, D.V. and Veda Bhanu, G. (2001), "Design, development and testing of Savonius wind turbine rotor with twisted blades", *Proceedings of the 28th National Conference on Fluid Mechanics and Fluid Power*, Chandigarh, India.

Gupta, R., Biswas, A. and Sharma, K.K. (2008), "Comparative study of a three-bucket Savonius rotor with a combined three-

bucket Savonius–three-bladed Darrieus rotor", *Renew. Energ.*, **33**, 1974-1981.

Hayashi, T., Li, Y., Hara, Y. and Suzuki, K. (2005), "Wind tunnel tests on a three-stage out-phase 2 Savonius rotor", *JSME Int. J.*, **48**(1), 9-16.

Ishimatsu, K., Kage, K. and Okubayashi, T. (2002), "Numerical study for the flow fields and performances of Savonius-type and Bach-type rotors", *Proceedings of the 10th International Symposium on Flow Visualization*, Kyoto Japan.

Kacprzak, K., Liskiewicz, G. and Sobczak, K. (2013), "Numerical investigation of conventional and modified Savonius wind turbines", *Renew. Energ.*, **60**, 578-585.

Kamoji, M.A., Kedare, S.B. and Prabhu, S.V. (2008), "Experimental investigations on single stage modified Savonius rotor", *Appl. Energ.*, **86**, 1064-1073.

Lee, J.H., Lee, Y.T. and Lim, H.C. (2016), "Effect of twist angle on the performance of Savonius wind turbine", *Renew. Energ.*, **89**, 231-244.

Mohamed, M.H., Janiga, G., Pap, E. and Thevenin, D. (2010), "Optimization of Savonius turbines using an obstacle shielding there turning blade", *Renew. Energ.*, **35**, 2618-2626.

Nasef, M.H., El-Askary, W.A., AbdEL-hamid, A.A. and Gad, H.E. (2013), "Evaluation of Savonius rotor performance: Static and dynamic studies", *J. Wind Eng. Ind. Aerod.*, **123**, 1-11.

Ross, I. and Altman, A. (2011), "Wind tunnel blockage corrections: review and application to Savonius vertical-axis wind turbines", *J. Wind Eng. Ind. Aerod.*, **99**(5), 523-38.

Saha, U.K. and Rajkumar, M.J. (2006), "On the performance analysis of savonius rotor with twisted blades", *Renew. Energ.*, **31**, 1776-1788.

Saha, U.K., Thotla, S. and Maity, D. (2008), "Optimum design configuration of Savonius rotor through wind tunnel experiments", *J. Wind Eng. Ind. Aerod.*, **96**, 1359-1375.

Sharma, S. and Kumar Sharma, R. (2017), "CFD investigation to quantify the effect of layered multiple miniature blades on the performance of Savonius rotor", *Energ. Convers. Manage.*, **144**, 275-285.

Tahania, M., Rabbani, A., Kasaeian, A., Mehrpooya, M. and Mirhosseinib, M., (2017), "Design and numerical investigation of Savonius wind turbine with discharge flow directing capability", *Energy*, **130**, 327-338.

Tong, Z. and Dietmar, R. (2013), "Numerical study of detailed flow field and performance of Savonius wind turbines", *Renew. Energ.*, **51**, 373-381.

CC

Nomenclature

Notations

A rotor swept area (m^2)

D rotor diameter (m)

D_m modified rotor diameter (m)

D_o end plate diameter (m)

d rotor blade diameter (m)

e gap distance between the rotor blades (m)

H rotor height (m)

L length of extension plate (m)

V wind speed (m/s)

y^+ dimensionless distance to the wall

w angular speed of water (rad/s)

C_p power coefficient

C_{ts} static torque coefficient

T_s static torque (Nm)

T dynamic torque (Nm)

B_R blockage ratio

S_a maximum projected area of the rotor (m^2)

T_a cross-sectional area of the wind tunnel (m^2)

Greek letters

λ rotor end speed ratio

θ angle of rotor (°)

ρ density (kg/m^3)

Abbreviations

3D   Three dimensional

ABS Acrylonitrile butadiene styrene

CAD Computer-aided design

CFD Computational fluid dynamics

FDM Fused deposition modeling

PLA Poly lactic acid